Inorganic Chemistry

Article

pubs.acs.org/IC

Triazolyl–Based Copper–Molybdate Hybrids: From Composition Space Diagram to Magnetism and Catalytic Performance

Ganna A. Senchyk,[†] Andrey B. Lysenko,*[,†] Artem A. Babaryk,[†] Eduard B. Rusanov,[‡] Harald Krautscheid,[§] Patrícia Neves,[∥] Anabela A. Valente,[∥] Isabel S. Gonçalves,[∥] Karl W. Krämer,[⊥] Shi-Xia Liu,*[,⊥] Silvio Decurtins,[⊥] and Konstantin V. Domasevitch[†]

[†]Inorganic Chemistry Department, Taras Shevchenko National University of Kyiv, Volodimirska Str. 64, Kyiv 01033, Ukraine

[‡]Institute of Organic Chemistry, Murmanska Str. 5, Kyiv 02660, Ukraine

[§]Institut für Anorganische Chemie, Universität Leipzig, Johannisallee 29, D-04103 Leipzig, Germany

[∥]Department of Chemistry, CICECO, University of Aveiro, Campus Universitário de Santiago, 3810-193 Aveiro, Portugal

[⊥]Departement für Chemie und Biochemie, Universität Bern, Freiestrasse 3, CH-3012 Bern, Switzerland

Supporting Information

ABSTRACT: The multicomponent mixed-metal Cu^{II}/Mo^{VI} oxides/1,3-bis(1,2,4-triazol-4-yl)adamantane (tr_2ad) system was thoroughly studied employing a compositional diagram approach. The concept allowed us to prepare three layered copper–molybdate hybrid solids $[Cu^{II}_2(tr_2ad)_4](Mo_8O_{26})$ (**1**), $[Cu^{II}_4(\mu_4\text{-}O)(tr_2ad)_2(MoO_4)_3]\cdot 7.5H_2O$ (**2**), and $[Cu^{I}_2(tr_2ad)_2](Mo_2O_7)\cdot H_2O$ (**3**), and to elucidate the relationship between initial reagent concentration/stoichiometry and the stability of the resultant structural motifs. Compounds **1** and **2** were found to dominate throughout a wide crystallization range of the concentration triangle, whereas compound **3** was formed by redox processes in the narrow crystallization area having a high excess of $Cu(OAc)_2\cdot H_2O$. Independent experiments carried out with $Cu(OAc)_2$ and $(NH_4)_6Mo_7O_{24}$ in the absence of tr_2ad, under the same conditions, revealed the formation of low-valent and bimetallic oxides, including Cu_2O, MoO_2, $Cu(Mo_3O_{10})\cdot H_2O$, and $Cu_3(MoO_4)_2(OH)_2$. Compounds **1** and **2** show high thermal and chemical stability as examined as catalysts in the epoxidation of *cis*-cyclooctene and the oxidation of benzyl alcohol (BzOH) with different types of oxidants. The oxidation reaction of BzOH using *tert*-butyl hydroperoxide (TBHP) as the oxidant, in the presence of **1** or **2**, led to benzaldehyde and benzoic acid ($PhCO_2H$), with the latter being formed in up to 90% yield at 24 h. The results suggest that **1** and **2** may be favorable heterogeneous catalysts for the synthesis of $PhCO_2H$. Whereas compound **1** only reveals a weak ferromagnetic coupling between neighboring Cu^{II} centers (J = 0.41 cm^{-1}), compound **2** shows distinct intracluster antiferromagnetic exchange interactions (J = −29.9 cm^{-1}, J' = −25.7 cm^{-1}), which consequently results in a diamagnetic ground state.

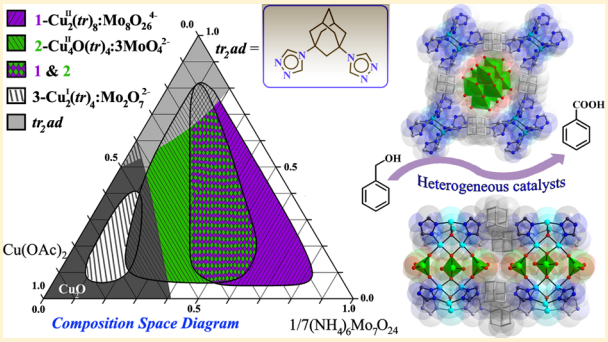

INTRODUCTION

The synthesis of organic–inorganic hybrids using hydrothermal conditions has received special attention in the field of coordination solids based on early transition-metal oxides, such as transition-metal molybdate complexes.[1] One reason for its popularity comes from the fact that a tremendous structural diversity of materials is readily accessible by the exploitation of the simplicity of the hydrothermal technique with various N-donor heterocyclic derivatives (bipy,[2] phen,[3] 1,2,4-triazole,[4] etc.). In the synthetic ocean of organic compounds and the crystal structures of the hybrid solids, it is easy to miss an intimate relationship between the organic ligand and inorganic-oxide reagents. In most cases, the importance of the interplay between initial reagent concentration and stoichiometry has not been addressed or discussed. In this context, the composition space diagram is a useful tool that allows synthetic pathways to be rationalized and to move one step closer toward the deep analysis of many reaction systems. The concept was successfully applied by Poeppelmeier et al. for the synthesis of pyridine-containing mixed-metal oxyfluorides[5] and silver vanadium oxide/oxyfluoride materials.[6] Similarly, a couple of recently published studies considered fluoride/oxyfluoride coordination solids with some other N-donor heterocycles acting in monodentate, chelating, or bridging modes (pyrazole, 2,2′-bipy, 4,4′-bipy, 1,2,4-triazole, etc.[7,8]). The application of this method toward uranium(VI) isonicotinate framework solids[9a] and some organically templated uranium(VI) sulfates[9b,c] was demonstrated by O'Hare et al. More recently, compositional diagrams constructed for M^{II}/1,2-di(4-pyridyl)ethane/$NaVO_3$

Received: April 30, 2014
Published: September 10, 2014

   dx.doi.org/10.1021/ic5009736 | Inorg. Chem. 2014, 53, 10112–10121

(M = Ni, Co) systems helped to elucidate qualitative crystallization sequences for a series of transition-metal vanadate hybrids.[10]

Though the approach can be considered as a general synthetic strategy for materials chemistry, many organic–inorganic systems, like polyoxomolybdates, in this sense are still largely unexplored and require a new methodological look. The high interest in the chemistry of molybdenum-oxide coordination solids, as fascinating materials in the fields of catalysis, magnetism, sorption, etc.,[11] stimulated our ongoing interest in the design of molybdenum(VI) oxide–organic frameworks (MOOFs)[12] and their oxyfluoride analogues[13] employing 1,2,4-triazolyl tectons. In this article we introduce our findings concerning the study of the mixed-metal $Cu^{I,II}$–Mo^{VI} oxides/bitopic 1,2,4-triazolyl ligand system using the compositional diagram screen with a further extension to a magnetic study and catalytic investigation for the epoxidation of *cis*-cyclooctene and the oxidation of benzyl alcohol (BzOH). The chosen metal–ligand combination possesses many attractive features. First, the ability of 1,2,4-triazoles to generate a short [N–N] link between two metal centers, a significant advantage in comparison with 4,4′-bipy, allows primary formation of coordinatively unsaturated clusters (Lewis acid sites) of desirable and stable configurations, such as linear $\{Cu_3[N–N]_{3+n}\}$, triangular $\{Cu_3(\mu_3\text{-}OH)[N–N]_3\}$, etc.[14] Employing a bitopic ligand like 1,3-bis(1,2,4-triazol-4-yl)adamantane (tr_2ad) produces metal–organic networks incorporating Cu^{II} redox clusters as secondary building units (SBUs).[15] The sterically bulky adamantane spheres increase the spacing between SBUs and simultaneously prevent the possible interpenetration of the networks. The steric environments provided by the hydrocarbon linkers can be regarded as a key factor to induce some specific hydrophobic interactions, protecting the Cu^{II}/Mo^{VI} redox centers from decomposition processes that would be undesirable in the context of further catalytic performance. On the other hand, the investigation of magnetic exchange interactions in polynuclear coordination compounds is a very topical issue in the field of molecular magnetism.[16]

EXPERIMENTAL SECTION

Measurements. Elemental analysis was carried out with a Vario EL-Heraeus microanalyzer. IR-spectra (400–4000 cm^{-1}) were obtained using a PerkinElmer FTIR spectrometer and KBr pellets. The room temperature (rt) powder X-ray diffraction patterns were measured out using a Stoe STADIP (Cu Kα1, using a linear PSD detector) and a Shimadzu XRD-6000 (Cu Kα). The temperature dependent X-ray measurements were recorded on a Stoe STADIP with a high temperature attachment and an image plate detector system. Simultaneous thermogravimetric/differential thermal analysis/mass spectrometry (TG/DTA-MS) studies were carried out on a Netzsch F1 Jupiter device connected to an Aeolos mass spectrometer. The sample was heated at a rate of 10 K min^{-1}. Magnetic susceptibility data were recorded using a Quantum design MPMS-5XL SQUID magnetometer in the temperature range 300–1.9 K and at a field of 2 kG. Experimental data were corrected for sample holder, diamagnetic contributions ($-0.45 \times$ molecular weight $\times 10^{-6}$ cm^3 mol^{-1}), and TIP contribution for Cu^{II} (60×10^{-6} cm^3 mol^{-1}).

X-ray Crystallography. The diffraction data were collected with graphite-monochromated Mo Kα radiation (λ = 0.710 73 Å). Measurements for **1** at 213 K and for **2** and $Cu_3(MoO_4)_2(OH)_2$ **4** at 296 K were performed on a Bruker APEXII CCD area-detector diffractometer (ω scans). The data were corrected for Lorentz-polarization effects and for the effects of absorption (multiscans method). Measurements for **3** at 213 K were made using a Stoe Image Plate Diffraction System, φ oscillation scans (numerical absorption correction using X-RED and X-SHAPE).[17] The structures were solved by direct methods and refined by full-matrix least-squares on F^2 using the SHELX-97 package.[18] The CH-hydrogen atoms were added geometrically, with $U_{iso} = 1.2U_{eq}$(C) and OH-hydrogen atoms, in **3** and **4**, located and included with fixed d(O–H) = 0.85 Å and $U_{iso} = 1.5U_{eq}$(O). For **2**, three MoO_4^{2-} anions constituting the environment of the $[(\mu_4\text{-}O)Cu_4]$ cluster are disordered over four positions, in such a way that the anions referenced by Mo2 and Mo3 atoms are ordered and two anions (Mo1 and Mo4) are equally disordered by symmetry over two positions (overlapping with the disordered solvate water molecules). All atoms corresponding to these MoO_4^{2-} anions were refined anisotropically, while oxygen atoms of the disordered water molecules were left isotropic and the corresponding hydrogen atoms were not added. For **1**, soft similarity restraints were applied to anisotropic thermal values of the atoms of one triazole ring. Graphical visualization of the structures was made using the program Diamond 2.1e.[19]

Crystallographic data and experimental details for structural analyses are summarized in Supporting Information Table S1. The crystallographic material can also be obtained from the CCDC, the deposition numbers being CCDC 981635–981638 for **1**–**4**, respectively.

Catalytic Tests. The catalytic oxidation reactions of *cis*-cyclooctene (Cy, 95%, Aldrich), benzaldehyde (≥99%, Aldrich), and benzyl alcohol (BzOH, anhydrous, 99.85%, Aldrich) were performed in 5 mL borosilicate batch reactors (equipped with a PTFE-lined magnetic stirring bar and a valve for sampling), under autogenous pressure, using an initial molybdenum/substrate/oxidant molar ratio of 1:100:153 (18 μmol Mo), and 1 mL of cosolvent [trifluorotoluene (TFT, anhydrous, 99%, Sigma-Aldrich), toluene (Tol, anhydrous, 99.8%, Scharlau), or CH_3CN (99.3%, Aldrich)], using predried *tert*-butyl hydroperoxide (TBHP, 5–6 M in decane, Aldrich) or H_2O_2 (30 wt % aqueous solution, Aldrich) as oxidant. TBHP was dried using activated 3 Å molecular sieves.

The procedure for starting the catalytic reaction involved charging the reactor with catalyst, substrate, and cosolvent, and then immersing the reactor into a thermostated oil bath at 75 °C, where it was kept under stirring (1000 rpm) for 10 min to attain isothermal initial conditions. Subsequently, the oxidant, also preheated at 75 °C, was added to the reactor, and this was taken to be the initial instant of the reaction. As an alternative to the hydroperoxide oxidants, molecular oxygen was used as the sole oxidant; the reactor was purged with O_2 and closed at ca. 1 bar pressure.

The contact tests were carried out as follows: the catalyst, cosolvent, and oxidant were charged to a reactor, and heated at 75 °C for 24 h with stirring at 1000 rpm. Afterward, the mixture was cooled to room temperature and centrifuged (3500 rpm), and the liquid phase was separated using a filter containing a 0.2 μm PTFE membrane. The liquid phase was transferred to a separate reactor, and preheated at 75 °C for 10 min. Finally, the substrate (also preheated) was added in an appropriate amount to obtain a similar initial concentration as that used for the typical reaction conditions (Mo/substrate/oxidant molar ratio of 1:100:153). The obtained solid was washed with pentane and vacuum-dried (ca. 0.1 bar) at 75 °C for 1 h, giving **1**-S and **2**-S from **1** and **2**, respectively. Catalytic tests were carried out for **1**-S and **2**-S using the typical reaction conditions.

The evolution of the catalytic reactions was monitored using a Varian 3900 GC equipped with a FID detector and a capillary column (J&W Scientific DB-5, 30 m × 0.25 mm × 0.25 μm), and calibration curves were measured using commercial standards. The reaction products were identified by GC–MS (Trace GC 2000 Series Thermo Quest CE Instruments GC; Thermo Scientific DSQ II), using He as the carrier gas.

Synthesis of the Coordination Compounds. All chemicals were of reagent grade and used as received without further purification. 1,3-Bis(1,2,4-triazol-4-yl)adamantane (tr_2ad) was prepared according to a previously described procedure.[15a]

*$[Cu_2(tr_2ad)_4](Mo_8O_{26})$ (**1**).* A mixture of $Cu(OAc)_2{\cdot}H_2O$ (10.0 mg, 0.050 mmol), tr_2ad (27.0 mg, 0.10 mmol), and $(NH_4)_6Mo_7O_{24}{\cdot}4H_2O$ (61.8 mg, 0.050 mmol) in 5 mL of water (molar ratio $Cu^{II}/tr_2ad/Mo^{VI}$

dx.doi.org/10.1021/ic5009736 | Inorg. Chem. 2014, 53, 10112–10121

= 1:2:7) was intensively stirred for a few minutes in a 20 mL Teflon-lined autoclave before being sealed. The autoclave was heated up to 160 °C, held for 24 h, and slowly cooled at 2.7 °C/h to rt. The monophasic violet needles were isolated in 45.0 mg yield (75%). Anal. Calcd for $C_{56}H_{72}Cu_2Mo_8N_{24}O_{26}$: C, 28.12; H, 3.03; N, 14.05. Found: C, 27.82; H, 2.94; N, 14.03. EDS analysis, atom % found: Cu, 19.42; Mo, 80.58. Calcd for Cu_2Mo_8: Cu, 20; Mo, 80. IR (KBr discs, selected bands, cm^{-1}): 409w, 475w, 514w, 546w, 640w, 660m, 703s, 729m, 843m, 876m, 1075m, 1112w, 1203m, 1324w, 1364w, 1458w, 1529m, 1630w, 1726w, 2867m, 2912m, 2942m, 3107m, 3142m, 3434w.

*$[Cu_4(\mu_4\text{-}O)(tr_2ad)_2(MoO_4)_3]\cdot 7.5H_2O$ (**2**).* A mixture of $Cu(OAc)_2\cdot H_2O$ (50.0 mg, 0.25 mmol), *tr_2ad* (27.0 mg, 0.10 mmol), $(NH_4)_6Mo_7O_{24}\cdot 4H_2O$ (26.5 mg, 21.4 μmol) in 5 mL of water (molar ratio $Cu^{II}/tr_2pr/Mo^{VI}$ = 5:2:3) was intensively stirred at rt for a few minutes in a 20 mL Teflon-lined autoclave before being sealed. A thermal treatment identical to that used for compound **1** was set up. The almost pure green product was isolated in 50.0 mg yield (70%). Anal. Calcd for $C_{28}H_{51}Cu_4Mo_3N_{12}O_{20.5}$: C, 23.59; H, 3.61; N, 11.79. Found: C, 23.91; H, 3.47; N, 11.84. EDS analysis, atom % found: Cu, 56.14; Mo, 43.86. Calcd for Cu_4Mo_3: Cu, 57.14; Mo, 42.86. IR (KBr discs, selected bands, cm^{-1}): 469w, 508w, 550m, 656m, 731w, 864vs, 1076m, 1204m, 1331m, 1366m, 1531m, 1636w, 2862w, 2934m, 3105m, 3400s.

*$[Cu_2(tr_2ad)_2](Mo_2O_7)\cdot H_2O$ (**3**).* A mixture of $Cu(OAc)_2\cdot H_2O$ (70.0 mg, 0.35 mmol), *tr_2ad* (27.0 mg, 0.10 mmol), and $(NH_4)_6Mo_7O_{24}\cdot 4H_2O$ (8.8 mg, 7.1 μmol) in 5 mL of water (molar ratio $Cu^{II}/tr_2pr/Mo^{VI}$ = 7:2:1) was intensively stirred at rt for a few minutes in a 20 mL Teflon-lined autoclave before being sealed. A thermal treatment identical to that used for compound **1** was set up. The resultant reaction mixture contained a brown powder of Cu_2O (a major phase) and colorless prisms (a minor phase) of the desired product. The crystals of **3** were separated from the inorganic Cu_2O solid in a $CHBr_3/CHCl_3$ solvent mixture on the basis of their different density (~6.0 g cm^{-3} for Cu_2O vs ~1.96 g cm^{-3} for **3**). The isolated product (~30% yield) contained a brownish amorphous contaminant covering the majority of crystals, which was not possible to separate by washing with solvents. Thus, single crystals were manually isolated for analysis. Anal. Calcd for $C_{28}H_{38}Cu_2Mo_2N_{12}O_8$: C, 33.98; H, 3.87; N, 16.98. Found: C, 34.08; H, 3.76; N, 17.02. IR (KBr discs, selected bands, cm^{-1}): 472w, 638m, 662m, 749s, 885s, 1040w, 1075w, 1111m, 1196w, 1294m, 1328m, 1360m, 1463m, 1535m, 1651m, 1745w, 2863s, 2915s, 3103s, 3427s.

Powder X-ray diffraction and inspection of the samples under a microscope were used to identify the products and to confirm their purity (see also Supporting Information Figures S20–S27).

RESULTS AND DISCUSSION

Synthesis and Composition Space Diagram. The copper–molybdate family of inorganic solids constitutes a remarkable variety of structures reflecting the unique relationship between the different coordination geometries accessible for $Cu^{I,II}$ and Mo^{VI} atoms as well as their diverse polyhedral connectivities.[20] We performed several hydrothermal experiments aimed at understanding the interactions between simple inorganic salts, $Cu(OAc)_2\cdot H_2O$ and $(NH_4)_6Mo_7O_{24}\cdot 4H_2O$, used in different proportions and concentrations under hydrothermal conditions. For instance, pure monocrystalline lindgrenite, $Cu_3(MoO_4)_2(OH)_2$ (monoclinic),[20g] was prepared by use of the reagents in a ratio of Cu^{II}/Mo^{VI} = 1:1 (0.06 M Cu^{II}). When excess of Mo^{VI} was present (e.g., Mo^{VI}/Cu^{II} = 8:1, 0.02 M Cu^{II}), the reaction proceeded to the isolation of green crystals of lindgrenite containing a trace contaminant of its polymorph (**4**) that crystallizes in the triclinic space group $P\bar{1}$ (a = 5.3507(2) Å, b = 5.5765(3) Å, c = 7.6182(4) Å, α = 103.810(3)°, β = 106.336(3)°, γ = 97.228(3)°, V = 207.24(3) Å^3).[20d] However, in the case of an 8-fold $Cu(OAc)_2$ excess (0.16 M Cu^{II}), the hydrothermal reaction yields almost pure red-brownish cuprous oxide (Cu_2O, $Pn\bar{3}m$),[21] which was identified by XRPD measurements (see the Supporting Information for details). At higher concentrations of $Cu(OAc)_2\cdot H_2O$ and $(NH_4)_6Mo_7O_{24}\cdot 4H_2O$, 0.48 versus 0.085 M, respectively, the formation of reduced molybdenum species (MoO_2 tugarinovite) together with $Cu(Mo_3O_{10})\cdot H_2O$[20i] and $Cu_3(MoO_4)_2(OH)_2$ (lindgrenite) was observed (Supporting Information Figures S15–S17).

N-donor heterocyclic ligands introduced as "a third component" into the reaction system generate a tremendous structural variety of copper–molybdate–organic hybrids. While optimizing hydrothermal conditions for such a complicated $Cu^{II}/tr_2ad/Mo^{VI}$ system, we screened a few inorganic salts, such as $Cu(OAc)_2\cdot H_2O$, $CuSO_4\cdot 5H_2O$, MoO_3, and $(NH_4)_6Mo_7O_{24}\cdot 4H_2O$. For instance, using $Cu(OAc)_2\cdot H_2O$ in combination with MoO_3 did not lead to any monocrystalline product, whereas the $CuSO_4\cdot 5H_2O/MoO_3$ pair gave a mixture of $[Cu_2(tr_2ad)_4](Mo_8O_{26})$ (**1**) and recently described Cu^{II} sulfate complexes.[15c] A combination of $Cu(OAc)_2\cdot H_2O$ and readily soluble $(NH_4)_6Mo_7O_{24}$ $4H_2O$ was found to be the most appropriate, and the temperature of 160 °C was the most convenient in the preparation of three new organic–inorganic hybrids, $[Cu_2(tr_2ad)_4](Mo_8O_{26})$ (**1**), $[Cu_4(\mu_4\text{-}O)(tr_2ad)_2(MoO_4)_3]\cdot 7.5H_2O$ (**2**), and $[Cu_2(tr_2ad)_2](Mo_2O_7)\cdot H_2O$ (**3**). Some initial attempts with intuitive proportions and concentrations were unsuccessful due to the formation of an unseparable mixture of violet and green crystalline phases **1** and **2**, respectively (Supporting Information Figure S20). Therefore, we decided to establish a composition space diagram to understand the interplay between organic and inorganic components under hydrothermal conditions. For the $Cu(OAc)_2\cdot H_2O/tr_2ad/(NH_4)_6Mo_7O_{24}\cdot 4H_2O$ system the composition triangle (Figure 1) was constructed by applying different molar ratios of the reactants from 1 to 8 (0.01–0.08 M Cu^{II}), so that 36 points were sequentially and systematically investigated (see more details in Supporting Information Table S9).

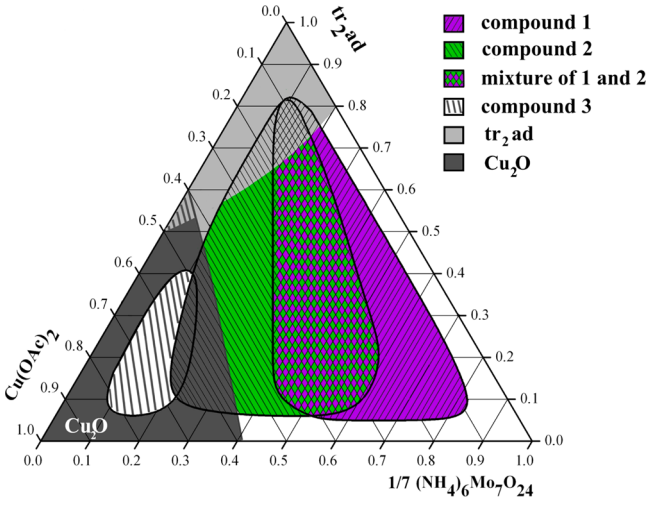

Figure 1. Composition space diagram for the $Cu(OAc)_2\cdot H_2O/tr_2ad/(NH_4)_6Mo_7O_{24}\cdot 4H_2O$ system showing crystallization areas of hybrids **1**–**3**.

All reactions were carried out using in the same quantity of water (5 mL). The consistency of either sample point was visually estimated and defined by XRPD, confirming that the amount of amorphous species as byproducts was mostly

dx.doi.org/10.1021/ic5009736 | Inorg. Chem. 2014, 53, 10112–10121

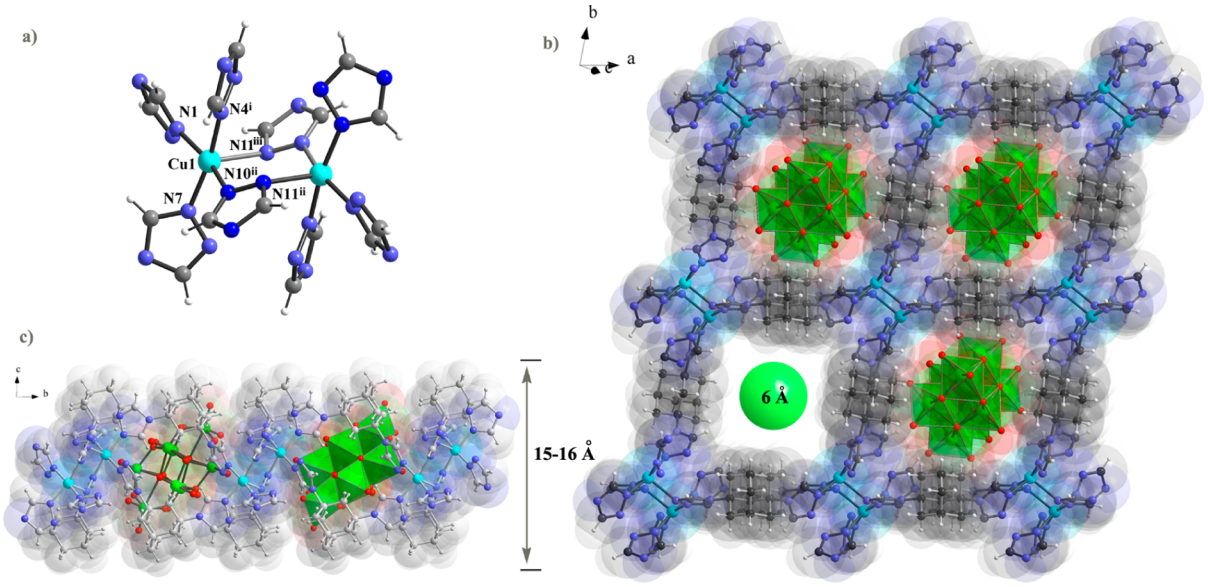

Figure 2. (a) Square-pyramidal coordination environment of copper centers in the $[Cu_2(\mu_2\text{-}tr)_2(tr)_6]$ SBU in **1**. The six-membered Cu1[−N−N−]$_2$−Cu1 metallоring adopts a chair conformation with maximum deviation of Cu1 atoms from the mean plane $N10^{ii}$−$N11^{ii}$−$N10^{iii}$−$N11^{iii}$ of *ca.* 0.78 Å. (b) The dinuclear units are interlinked into a 2D network which accommodates β-$Mo_8O_{26}^{4-}$ anions, viewed along the $[\bar{3}51]$ direction. (c) The large bulky adamantane scaffold introduced in the ligand structure provides an increased layer thickness of ca. 15−16 Å. Symmetry codes in compound **1** follow: (i) $-x, 1-y, 2-z$; (ii) $1-x, 2-y, 2-z$; (iii) $-x+1, y, z$. Selected distances (Å) follow: Cu1−$N4^{i}$ 1.968(6), Cu1−N1 1.976(7), Cu1−N7 1.992(6), Cu1−$N10^{ii}$ 2.002(7), Cu1−$N11^{iii}$ 2.247(7).

Table 1. Principal Geometric Parameters Observed in the Crystal Structures of 1−3 (Å)

	1	2	3
SBU type	$[Cu^{II}_2(\mu_4\text{-tr})_2]$	$[Cu^{II}_4(\mu_4\text{-O})]$	$[Cu_2(\mu_4\text{-tr})_2]$
coord environment	$\{N_4+N\}$	$\{N_2O_3\}$	$\{N_3\}$
Cu−N, N^1,N^2-*tr*	2.002(7), 2.247(7)	2.005(8)−2.093(9)	1.938(3)−2.002(3)
Cu−N, terminal-*tr*	1.968(6)−1.992(6)		1.927(3)−1.934(3)
Cu−O (μ_4-oxo)		1.955(6)−1.966(9)	
Cu−O, $\mu_4\eta^2$ bridging $([MoO_4]^{2-})^a$		1.964(12), 2.028(14), 2.091(11)	
Cu−O, $\mu_2\eta^2$ bridging $([MoO_4]^{2-})^a$		1.924(9), 1.938(10)	
Cu···Cu (intra)	3.926	2.864, 2.946, 3.335, 3.340	3.540
closest intercluster distance^b	12.113	8.092	9.238

^{a}Disordered anions. ^{b}The value corresponds to the distance between geometric centers of the neighboring clusters ($\{Cu_4O\}$ or $\{Cu_2(tr)_2\}$).

neglectable. Thus, three distinct areas of selective crystal growth can be identified within the diagram (Figure 1). In the bottom right corner with a high excess of the molybdenum source (5−8 equiv) compound **1** predominantly forms, while for crystallization of **2** a significant excess of the Cu^{II}-component is needed. Both crystallization fields have a large overlapping area in the middle of the triangular diagram. Increasing the Cu^{II} molar ratio from 5 up to 8 equiv (bottom left corner) induced the decomposition of $Cu(OAc)_2{\cdot}H_2O$ to cuprous oxide, precipitating as a brownish fine powder, but simultaneously the coordination polymer of Cu^{I} (**3**) crystallizes as colorless blocks. The high concentration and up to 8-fold excess of ligand tr_2ad, that exhibits moderate solubility in water, facilitates its partial recrystallization, affording large colorless prisms of trihydrate $tr_2ad{\cdot}3H_2O$. Taking into account the resulting diagram we found the most appropriate conditions for the separate synthesis of pure phases **1** at a $Cu^{II}/tr_2ad/Mo^{VI}$ ratio of 1:2:7, and **2** at a $Cu^{II}/tr_2ad/Mo^{VI}$ ratio of 5:2:3.

Crystal Structures. The crystal structure of compound **1** consists of copper atoms in a $\{N_4+N\}$ square-pyramidal environment which is combined within a centrosymmetric dinuclear unit and supported by two μ_2-[N−N]-tr groups (Figure 2, Table 1). Among numerous bis-triazolyl ligand complexes with M^{2+} cations, the formation of such a cluster type having a double [−N−N−] bridge has rarely been observed, e.g., in $[Cu_2(btr)_4(NO_3)_2](NO_3){\cdot}2H_2O$ (*btr* = 4,4′-bi(1,2,4-triazole).[22,23] The most favorable examples include discrete triangular $\{M_3(\mu_3\text{-OH})[-N-N-tr]_3\}$, linear $\{M_2[-N-N-tr]_3\}/\{M_2(\mu_2\text{-X})[-N-N-tr]_2\}$ (X = Cl^-, F^-, NCS^-) clusters, and their oligomerized chain architectures.[14]

In complex **1**, the $[Cu_2(\mu_2\text{-}tr)_2(tr)_6]$ arrangement is completed by bi- and tridentate tr_2ad linkers in a ratio of 1:1 that provides long (12.113 and 12.763 Å) double-bridge connections between the secondary-building blocks running in two directions. Such ligand distributions result in the construction of microporous wall-like layered sieves that are built up from nanosized capsules of hydrophobic adamantane spacers. The cavities exist in a "double-cone" conformation, fused at the wider inside rim, exhibiting a small exterior aperture with a van der Waals cross-section of 6.0 × 6.0 $Å^2$ versus a large interior cross-section of around 9.0 × 10.0 $Å^2$ (Figure 2b,c). Despite the large hydrophobic surface of the hydrocarbon scaffolds, the internal cavities are perfectly suited to capture large hydrophilic β-$\{Mo_8O_{26}\}^{4-}$ anions. These

dx.doi.org/10.1021/ic5009736 | *Inorg. Chem.* 2014, 53, 10112−10121

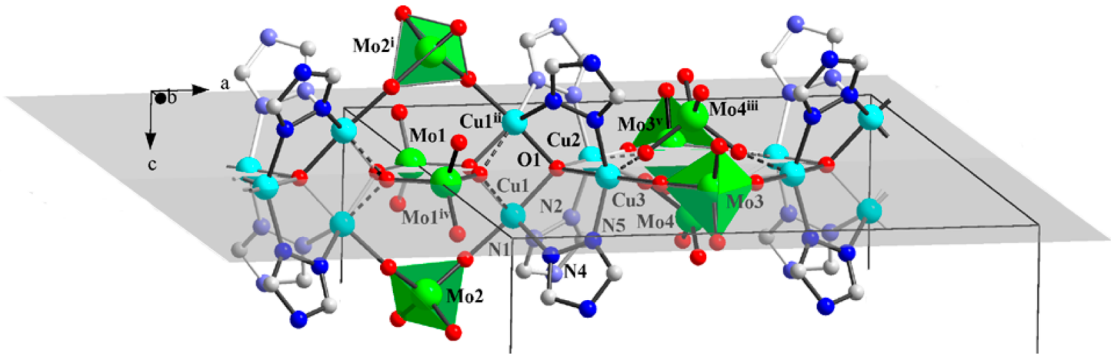

Figure 3. Unique combination of tetrahedral cationic $[Cu_4O]^{6+}$ clusters, MoO_4^{2-} anions, and [−N−N−] *tr* bridges for **2** leads to a column structural motif. Note that disordered Mo1 and Mo4 anions with a partial occupancy factor of 0.5 are represented in ball-and-stick mode, while the other molybdate anions are shown in polyhedral representation; the (110) plane bisects the structural motifs. (Crystallographic and refinement details are shown in Supporting Information.)

anions serve the charge-compensating role without any significant interactions with the Cu^{II} centers. Another factor that should be taken into account is the remarkable size- and shape-complementarity of the β-$\{Mo_8O_{26}\}^{4-}$ guests with the surrounding square grid adamantane-belt. These interactions are supported by a set of weak C−H···O hydrogen bonds (see Supporting Information, Figure S3). It is assumed that the material is not prone to anion exchange processes and thus can be regarded as a convenient heterogeneous catalyst. Despite the highly hydrophilic nature of β-$\{Mo_8O_{26}\}^{4-}$ anions, no water (solvent) molecules are present within the interlayer space. On the other hand, as shown before for coordination polymers $[Cu_3(tr_2ad)_4(H_2O)_4](SiF_6)_3\cdot 16H_2O$ and $[Cu_3(tr_2ad)_4(H_2O)_2(SO_4)_2]SO_4\cdot 28H_2O$,[15c] a related 2D square-grid architecture can store huge amounts of crystallized water molecules. Apparently, the hydrophilicity−hydrophobicity of the similar square-grid network $[Cu^{II}_2(tr_2ad)_4]_n$ can be tuned by introducing small or big counteranions, like small SiF_6^{2-} or SO_4^{2-} versus bulky $\{Mo_8O_{26}\}^{4-}$, respectively.

The layered-type structure of compound **2** can be regarded as built from the unusual combination of tetrahedral oxo-centered $[Cu_4O]^{6+}$ clusters, tetrahedral MoO_4^{2-}, and tr_2ad ligands taken in a ratio of 1:3:2 (Figure 3, Table 1). The configuration of the $[Cu_4O]$ core is supported by μ^2-[−N−N−] triazolyl linkages along four edges (Cu···Cu 3.335, 3.340 Å) while the other two edges of tetrahedra are spanned by MoO_4^{2-} anions (Mo1 and Mo4 centers) acting in a μ_4,η^2-bridging mode. Another kind of MoO_4^{2-} anion adopts a μ_2,η^2-coordination to double-bridge neighboring $[Cu_4O]$ clusters through two vertices. Two MoO_4^{2-} anions (Mo1 and Mo4) are disordered about the inversion center which is located between four molybdenum sites, Mo3 and Mo4, at (0.5, 0.5, 0) (Figure 3). This results in a statistical disorder of the MoO_4^{2-} species along the *a* axis so as to alternate the anions between the two orientations.

The presence of two kinds of ligands, neutral *tr*-groups on one hand, and inorganic anions located around the $[Cu_4O]$ core on the other hand, affords appreciably different Cu···Cu distances within the cluster (3.335, 3.340 vs 2.864, 2.946 Å for triazolyl and molybdate bridges, respectively) and is the reason for the geometric distortion of the $[Cu_4O]$ tetrahedra. The conformationally rigid angular tr_2ad ligand displays a uniform tetradentate coordination mode providing a 12.414 Å double-bridging interconnection between adjacent $[Cu_4O]$ SBUs. This leads to $[Cu_4O(tr_2ad)_2]$ chain motifs that run parallel to the *c* axis. In a perpendicular direction, molybdate tetrahedra as bi- and tridentate-bridging anions sew the $[Cu_4O]$ nodes together at a distance of 8.092 Å, thus resulting in further interconnection of the strands to a 2D network (Figure 4).

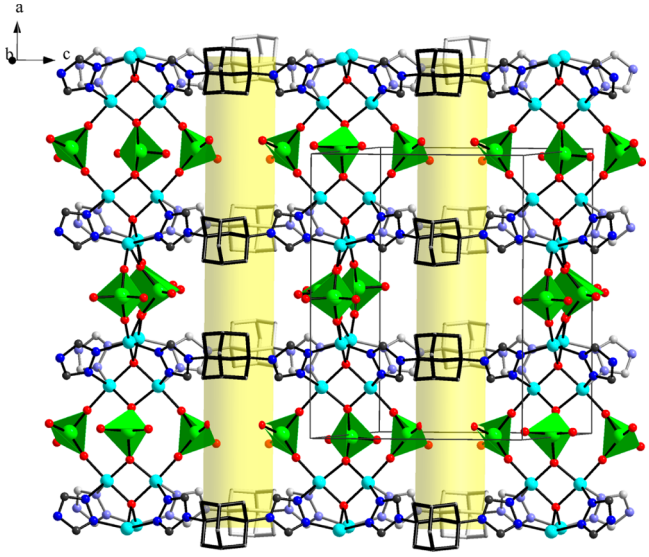

Figure 4. In the crystal structure of complex **2**, the tetrahedral $[Cu_4(\mu_4\text{-}O)]$ SBUs are linked by two sets of building blocks (MoO_4^{2-}, shown as tetrahedra, and tr_2ad) to form a 2D layer extending in the *ac* plane.

The neighboring layers shifted by $^1/_2a$ and $^1/_2c$ along the *a* and *c* axes, respectively, are stacked one over the other along the *b* axis (Figure 5). The uncoordinated water molecules fill the interlayer space forming H-bonding interactions with MoO_4^{2-} as the most hydrophilic H-bond acceptor sites.

The presence of excess of $Cu(OAc)_2$ and tr_2ad over the Mo^{VI} component led to isolation of the Cu^I complex $[Cu^I_2(tr_2ad)_2](Mo_2O_7)\cdot H_2O$ (**3**). As shown before, the formation of Cu^I triazolyl-based coordination polymers, to be prepared *in situ* from Cu^{II} sources, is quite common. Likely, the highly efficient electron-withdrawing nature of the triazolyl-ring facilitates the stabilization of the Cu^I oxidation state in aqueous medium even under quite severe hydrothermal conditions.[24] The asymmetric unit of compound **3** contains two copper atoms, two tr_2ad ligands, a solvate water molecule, and one dimolybdate anion (Figure 6). Each Cu^I atom adopts a distorted $\{N_3\}$

dx.doi.org/10.1021/ic5009736 | *Inorg. Chem.* 2014, 53, 10112−10121

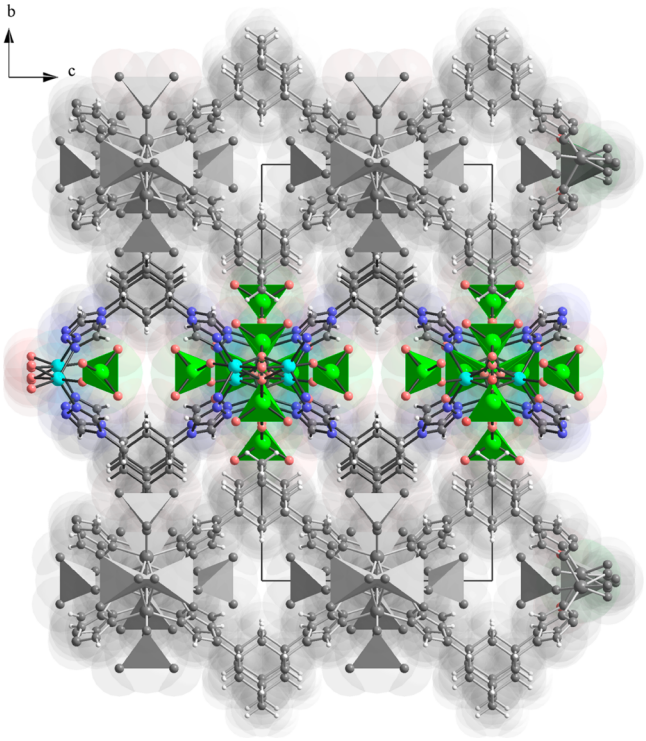

Figure 5. Undulating $[Cu_4(\mu_4\text{-}O)(tr_2ad)_2(MoO_4)_3]$ sheets of **2** are stacked in a parallel fashion along the *a* axis (MoO_4^{2-} presented as tetrahedra, whereas the solvent water molecules trapped within the layers are not shown).

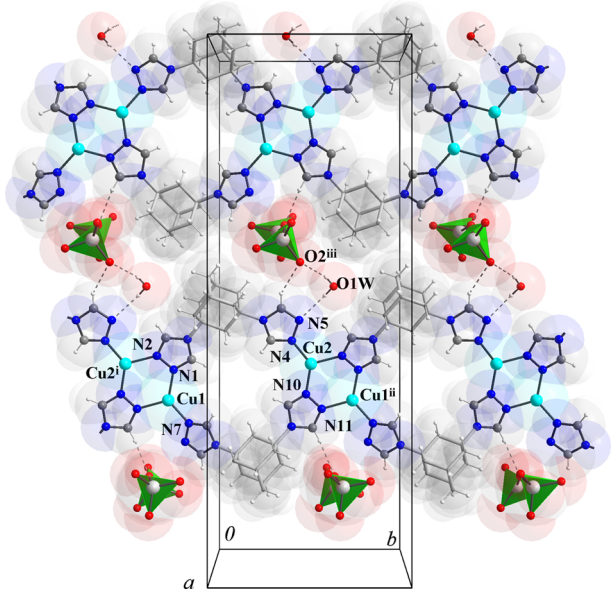

Figure 6. Projection of the crystal structure of $[Cu^I_2(tr_2ad)_2](Mo_2O_7)\cdot H_2O$ (**3**) in the *bc* plane showing a hydrogen-bonded layer (symmetry codes: (i) *x*, −1 + *y*, *z*; (ii) *x*, 1 + *y*, *z*; (iii) −0.5 + *x*, 0.5 − *y*, 1 − *z*).

coordination environment formed by tridentate tr_2ad ligands through a monocoordinating and two [−N−N−] bridging *tr* groups. This dinuclear structural motif dominates for Cu^I complexes with 1,2,4-trizolyl-based ligands,[24] and their AgI-anologues[15b,25] as well. A 1:1 metal-to-ligand ratio realized in complex **3** leads to a chain structure, running along the *b* axis, in which the $[Cu_2(\mu_2\text{-}tr)_2]^{2+}$ fragments as corners are double-bridged by tr_2ad at the distance of 11.513 Å, through angular adamantane spacers, to form open rhombic cavities (ca. 3.0 × 5.0 $Å^2$ in internal van der Waals cross-section). The small size of the cavity does not allow uncoordinating dioctamolybdate counterions to be incorporated which, therefore, occupy the interchain space aligning along the *a* axis. The location is stabilized by hydrogen bonding to the cocrystallized water molecule and to the (tr)C−H groups (see C−H···O(Mo) interactions, Supporting Information Figure 7.[26]

Thermal Stability. The thermal stability of compounds **1** and **2** was examined by temperature dependent powder X-ray diffractometry (TD PXRD) and thermogravimetric analysis (Supporting Information Figures S13 and S14). According to the data, compound **1** shows sufficient stability up to about 310 °C with the corresponding plateau region on the TG curve. Then, it exhibits a weight loss step attributed to the ligand oxidation process, which is accompanied by a release of volatile decomposition products, CO_2 (m/z = 44) and H_2O (m/z = 18).

Due to the presence of crystallization water molecules in the crystal structure of compound **2**, its thermal decomposition profile is significantly different from that of **1** (Supporting Information Figure S14a). A first weight loss occurring in the temperature interval 70−210 °C can be associated with removal of the solvent, whereas the second weight loss above 240 °C corresponds to the irreversible oxidation of the solid. More interesting details can be concluded from the corresponding TD PXRD pattern (Supporting Information Figure S14b). In the middle of the dehydration process (∼110−120 °C), most of the diffraction peaks are split or slightly shifted. This effect can be induced by distortions of the framework to lower symmetry because of the high sensitivity of the interlayer spacing toward guest removal. The high thermal stability of the layered structure can be confirmed by a series of IR measurements for the samples heated in air at temperatures of 70, 150 (the point, where the bifurcation effect is observed), 200, and 260 °C. As shown in Supporting Information Figure S11, except for the IR spectrum of the sample heated at 260 °C, no observable changes were detected in the 400−4000 cm^{-1} region. For the former, the appearance of the $\nu(C{\equiv}N)$ band at 2125 cm^{-1} reveals the irreversible decomposition of 1,2,4-triazole ligands. The experimental XRPD patterns s-70, s-150, s-200, which are identical to that of pure phase **2**, provide clear evidence that the dehydration processes below 200 °C are reversible. The data are in a good correlation with the Guinier−Simon diagram (Supporting Information Figure S14b) which provide evidence for the structural collapse of the framework above 210 °C.

Magnetic Studies. The extended network compounds **1** and **2** were studied by magnetic susceptibility measurements. The $\chi_m T(T)$ plot (Figure 7) of a polycrystalline sample of **1** exhibits essentially constant $\chi_m T$ values (0.85 cm^3 K mol^{-1}) on cooling from rt, which only increase slightly below 20 K to 0.99 cm^3 K mol^{-1} at 1.9 K. The high temperature $\chi_m T$ values compare well with the spin-only value for two noninteracting spins with $S = {}^1/_2$. The sparse increase of the $\chi_m T$ values at very low temperatures reflects some fairly weak ferromagnetic exchange interactions occurring within the structurally isolated dimeric Cu^{II} units. It can be deduced from the structural analysis (see Figure 2a) that the magnetic orbitals (orbital perpendicular to the Jahn−Teller axis of each copper center) of the two bridged Cu^{II} ions are situated in a parallel manner, which is not favorable for a remarkable magnetic exchange

dx.doi.org/10.1021/ic5009736 | Inorg. Chem. 2014, 53, 10112−10121

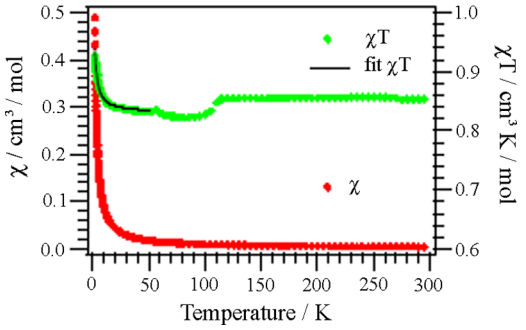

Figure 7. Thermal variation of χ_m and $\chi_m T$ for **1** (black line is a fit).

interaction, thus leading to the constant $\chi_m T$ values over a wide temperature range. The slight magnetic exchange interaction being visible at very low temperatures could be expected to be of ferromagnetic nature because the two triazole ligands bridge the magnetic orbitals of both paramagnetic centers in an orthogonal manner. A fit of the magnetic susceptibility data in the temperature range below 50 K with the Bleaney−Bowers equation results in the parameters J = 0.41 cm^{-1} and g = 2.10. The inverse magnetic susceptibility (χ_m^{-1}) versus T curve of **1** (Supporting Information Figure S30) shows a linear behavior, and a Curie−Weiss fit at temperatures above 150 K extrapolates to a zero Θ value, indicating at most only a minor magnetic exchange interaction within the dimeric units. In addition, although hardly visible in the $\chi_m(T)$ plot, there is a slight jump in the χ_m data around 110 K which is an intrinsic property of the compound, as it was confirmed by repeating measurements; it can likely be attributed to a structural phase transition.

In contrast to compound **1**, the magnetic study of compound **2** reveals a more pronounced temperature dependence of the magnetic susceptibility. Figure 8 shows the $\chi_m T(T)$ plot of a

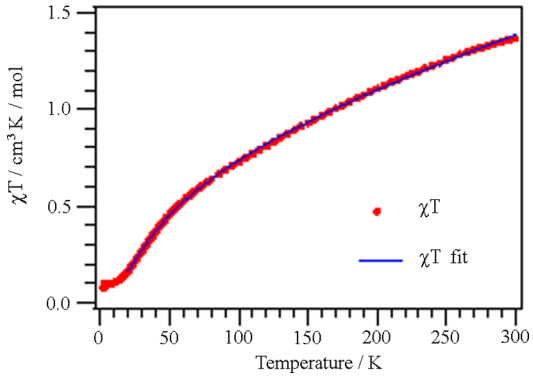

Figure 8. Thermal variation of $\chi_m T$ for **2** (solid line is a fit).

polycrystalline sample of **2** exhibiting a $\chi_m T$ value of 1.36 cm^3 K mol^{-1} at 300 K which gradually decreases while lowering the temperature. These data indicate that the tetranuclear Cu^{II} units exhibit a predominantly antiferromagnetic intracluster interaction; already the rt $\chi_m T$ value lies distinctly below the theoretical one for four noninteracting Cu^{II} centers (1.58 cm^3 K mol^{-1} with g = 2.1).

On the basis of the structural motif of the tetranuclear entity (Figure 3) we can use the following isotropic Hamiltonian to describe the intracluster magnetic exchange interactions (eq 1):

$$H = -2J(S_1 \cdot S_2 + S_1 \cdot S_3 + S_{1ii} \cdot S_2 + S_{1ii} \cdot S_3) - 2J'(S_1 \cdot S_{1ii} + S_2 \cdot S_3) \quad (1)$$

This model approximates the coupling interactions with only two parameters (J, J') which avoids an overparameterization. The energy parameter J reflects an exchange pathway comprising both bridges, namely through the μ^2-[−N−N−] triazolyl ligands and the μ^4-O bonding, whereas J' stands for the μ^4-O bond only. Consequently, the Hamiltonian gives rise to six spin states comprising the total spin values (S_T) of 2, 1, 0 with the corresponding energy levels in terms of the magnetic coupling constants J and J' as given below:[27]

$$E_1(S_T = 2) = -2J - J'$$

$$E_2(S_T = 1) = +2J - J'$$

$$E_3(S_T = 1) = +J'$$

$$E_4(S_T = 1) = +J'$$

$$E_5(S_T = 0) = +3J'$$

$$E_6(S_T = 0) = +4J - J'$$

Applying these energy values to the van Vleck equation[27] allows the fitting of the experimental data. For the temperature range above 20 K, the experimental magnetic susceptibility data were best represented by the values g = 2.1, J = −29.9 cm^{-1}, J' = −25.7 cm^{-1}; the excellent fit is shown in Figure 8. These parameters place the singlet states energetically below the triplet levels which conforms with the tendency of the experimental $\chi_m T$ values to approach a zero value at low temperature. The slight nonzero experimental values originate from a minor amount of a Curie-behaved paramagnetic impurity.

The peculiar bonding pattern within the tetranuclear Cu^{II} clusters, where μ^2-[−N−N−] triazolyl ligands are mixed with the tetrahedral μ^4-O bonding scheme, prevents a detailed structure−property correlation. At best, the chosen Hamiltonian reflects the approximated symmetry of the intracluster bonding pattern which essentially reveals two types of linkages among the four paramagnetic centers, both with reasonable and similar antiferromagnetic coupling strength.

Catalytic Studies. Molybdenum compounds may be promising catalysts for the epoxidation of olefins using hydroperoxides as oxidants, under relatively mild reaction conditions. The catalytic performances of **1** and **2** were first investigated in the epoxidation of *cis*-cyclooctene (Cy; model substrate) with *tert*-butylhydroperoxide (5−6 M in decane; TBHP), using trifluorotoluene (TFT) as cosolvent at 75 °C (using the catalysts in the same equivalent number of moles of molybdenum). The reaction was quite sluggish for **1** and **2**, giving 1,2-epoxycyclooctane (CyO) as the main product formed in ca. 12% and 23% yield, at 23% and 45% conversion (after 24 h reaction time), respectively. Besides CyO, the reaction products included cyclooctenones. Iodometric titrations carried out for the catalysts mixed with TBHP (without substrate, at 75 °C, 24 h) indicated considerable "nonproductive" decomposition of TBHP for **2**, and negligible TBHP decomposition in the case of **1**. These results may partly explain the poor oxidation activity of **2**, although this catalyst led to a higher reaction rate than **1**. These results suggest that the "nonproductive" decomposition of the oxidant becomes

dx.doi.org/10.1021/ic5009736 | Inorg. Chem. 2014, 53, 10112−10121

less important with the presence of the substrate, possibly via competitive adsorption effects on the catalyst's surface.

Molybdenum and copper catalysts may be interesting for the oxidation of alcohols. Mixtures of copper and molybdenum homogeneous catalysts have been successfully used for the oxidative dehydrogenation of BzOH to benzaldehyde (PhCHO), using molecular oxygen as oxidant, at approximately 1 atm and 100−111 °C (toluene as solvent).[28,29] Compounds **1** and **2** were further explored as catalysts for the liquid-phase oxidation of BzOH, using different types of oxidants. Compounds **1** and **2** were not active in the oxidation of BzOH (i) with O_2 using toluene (Tol) as cosolvent, or (ii) with aqueous H_2O_2 using acetonitrile as cosolvent, at 75 °C. In contrast, the reaction of BzOH using TBHP as oxidant, in the presence of **1** or **2**, led to PhCHO and benzoic acid ($PhCO_2H$), with the latter being formed in up to 90% yield at 24 h reaction. Benzoic acid is industrially produced for several applications, such as for food preservation compounds, drugs, fragrances, and flavors.[30,31]

The reaction of BzOH with TBHP, in the presence of **1** and **2**, using TFT as cosolvent, at 75 °C, led to PhCHO and $PhCO_2H$ as the main reaction products (Table 2). For the catalysts used in an equivalent amount of molybdenum, **1** led to slower reaction of BzOH than **2**; conversion at 4 h/24 h was 17%/85% and 59%/92% for **1** and **2**, respectively (entries 1 and 4, Table 2). This trend in reaction rates somewhat parallels that observed for Cy as substrate (discussed above). For **1** and **2**, PhCHO and $PhCO_2H$ yields at 24 h reaction were 16−26% and ca. 70%, respectively. These results indicate that **2** possesses superior catalytic performance in relation to **1** (based on similar mass of loaded catalyst). The byproducts included *tert*-butyl benzoate, which can result from the esterification reaction between benzoic acid and *tert*-butanol (a coproduct of the reaction of TBHP). The PhCHO selectivity tended to decrease with time, with the concomitant increase in $PhCO_2H$ selectivity. These results are consistent with PhCHO being an intermediate of the conversion of BzOH to $PhCO_2H$. Accordingly, the reaction of PhCHO in the presence of **2** led to $PhCO_2H$ as the only product formed in 67% yield at 100% conversion, reached at 24 h reaction.

Table 2. Catalytic Results for 1 and 2 Tested in Liquid-Phase Oxidation of Benzyl Alcohol at 75 °C[a]

				product selectivity at 1/4/24 h (%)	
entry	catalyst	solvent	conversion at 1/4/24 h (%)	PhCHO	$PhCO_2H$
1	**1**	TFT	1/17/85	100/100/26	0/0/70
2	**1**	TFT[b]	18/53/88	100/45/28	0/54/66
3	**1-S**	TFT	2/34/93	100/100/25	0/0/62
4	**2**	TFT	13/59/92	100/40/16	0/49/71
5	**2**	TFT[c]	59/86/100	100/26/0	0/61/90
6	**2**	Tol	10/55/81	100/49/25	0/41/65
7	**2-S**	TFT	10/53/89	100/49/13	0/49/66

[a]Reaction conditions: 1.1 M BzOH, TBHP/substrate/Mo molar ratios of 153:100:1, 75 °C. [b]TBHP/substrate/Cu molar ratios of 113:75:1. [c]Initial concentration of BzOH was 0.7 M (TBHP/substrate/Mo molar ratios of 153:64:1).

To the best of our knowledge, there is no report on the use of mixed molybdenum−copper heterogeneous catalysts for the reaction of BzOH with TBHP. A clear comparison of the catalytic results for **1** and **2** with the literature data for copper or molybdenum heterogeneous catalysts is complex, partly due to the differences in reaction conditions used. Nevertheless, **1** and **2** seem to be favorable catalysts for the synthesis of $PhCO_2H$ (Table 3).

Using complex **1** in an equivalent amount of copper as that used for **2** led to comparable catalytic results for the two catalysts (entries 2 and 4, Table 2). However, this corresponds to ca. 3.4 times more mass of catalyst **1** than of **2**, and a much higher amount of molybdenum added together with **1** than with **2**. These results suggest that the catalytic activity correlates essentially with the amount of copper sites. If the molybdenum sites were solely responsible for the catalytic reaction, then one would expect faster reaction for **1** than for **2**, which was not the case. Furthermore, on the basis of similar moles of molybdenum (discussed above), **1** led to poorer catalytic results than **2** which may be partly due to the higher amount of copper which was added with **2** than with **1** under these reaction conditions. These results suggest that the copper sites play an important catalytic role in the conversion of BzOH to $PhCO_2H$. This hypothesis is somewhat supported by the catalytic results for the reaction of BzOH, using the synthetic transition-metal precursors as (homogeneous) catalysts, namely $Cu(CH_3COO)_2{\cdot}H_2O$ (Cu/substrate molar ratio = 0.01) and $(NH_4)_6Mo_7O_{24}{\cdot}4H_2O$ (Mo/substrate molar ratio = 0.05). The molybdenum precursor exhibited poor activity and led to PhCHO as the main product (10% yield at 10% conversion, 24 h reaction) and $PhCO_2H$ was not formed. The copper precursor (used in considerably lower molar amount than the molybdenum precursor) led to faster reaction of BzOH than the molybdenum precursor, and $PhCO_2H$ was the main product (38% yield at 65% conversion, 4 h reaction). The metal precursors were further tested as catalysts in the reaction of PhCHO, under similar reaction conditions to those used for BzOH as substrate. The reaction of PhCHO in the presence of the molybdenum precursor was sluggish (30% conversion at 6 h, and $PhCO_2H$ was the only product), whereas the copper precursor led to $PhCO_2H$ with 72% yield at 98% conversion (6 h). On the basis of these results, one may postulate that the copper sites of **1** and **2** are more active than the molybdenum sites in the conversion of BzOH to $PhCO_2H$.

In the case of **2**, decreasing the initial concentration of BzOH from 1.1 to 0.7 M led to faster initial reaction (based on conversion at 1 h reaction), and 90% $PhCO_2H$ yield was reached at 100% conversion (entry 5, Table 2). Using Tol as cosolvent instead of TFT led to a slight decrease in reaction rate and $PhCO_2H$ selectivity at high conversion (entry 6, Table 2). The favorable effect of TFT as solvent may be partly related to its higher polarity favoring the catalytic reaction of the relatively polar reagents BzOH and TBHP.

The catalyst stability of **1** and **2** was investigated in the reaction of BzOH with TBHP, by performing contact tests (details given in the Experimental Section). The obtained solids (**1-S** and **2-S** for **1** and **2**, respectively) and liquid phases were tested in the reaction of BzOH with TBHP, during 24 h, at 75 °C (TFT as cosolvent). The liquid phases for **1** and **2** led to no measurable conversion of BzOH, suggesting the absence of soluble active species, and that **1** and **2** act as heterogeneous catalysts. **1-S** and **2-S** were characterized by FT-IR ATR, and their spectra were fairly similar to those of **1** and **2**, respectively (Supporting Information Figure S12), suggesting that these are fairly stable heterogeneous catalysts. The oxidation of BzOH with TBHP in the presence of **1-S** and **2-S** led to roughly the

dx.doi.org/10.1021/ic5009736 | Inorg. Chem. 2014, 53, 10112−10121

Table 3. Literature Data for Molybdenum and Copper Heterogeneous Catalysts Tested in the Liquid Phase Oxidation of Benzyl Alcohol with TBHP

catalyst	solvent; T (°C); time (h)	TBHP/BzOH/M[a]	conv (%)	product selectivity (%) PhCHO	product selectivity (%) $PhCO_2H$	ref
$[Mo(CO)_6]$ supported on multiwall carbon tubes	CCl_4; 72; 1	133:67:1*[b]	100	60	40	32
spinel Cu,Fe	CH_3CN; 60; 4	20:20:1**	~25	~60	~40	33
spinel Cu,Cr	CH_3CN; 60; 4	20:20:1**	~15	~60	~40	33
Cu,Co oxides	CH_3CN; 60; 4	20:20:1**	~15	~96	n.m.[c]	33
Cu,Cr oxides	CH_3CN; 60; 4	20:20:1**	~29	~70	n.m.[c]	33
Cu,Fe oxides	CH_3CN; 60; 4	20:20:1**	~22	~87	n.m.[c]	33
spinel Cu,Co	CH_3CN; 60; 4	20:20:1**	~19	~84	n.m.[c]	33
spinel Cu,Cr	CH_3CN; 60; 4	20:20:1**	~10	~99	n.m.[c]	33
8% poly(*S*-DVB)-L-valine Cu(II) complex[d]	CH_3CN; 45; 24	136:91:1*	75	96	n.m.[c]	34
6% Poly(S-DVB)-L-valine Cu(II) complex[d]	CH_3CN; 45; 24	133:88:1*	73	96	n.m.[c]	34
PS−$(PBIM)_2$Cu(II)[e]	CH_3CN; 70; 0.05	250:250:1*	94	93	n.m.[c]	35
PS−$(QBIM)_2$Cu(II)[e]	CH_3CN; 70; 3	250:250:1*	91	98	2	36
Cu(II)−NaY	CH_3CN; 75 ; 6	200:100:1*	38	31	69	37
CuL−NaY[f]	CH_3CN; 75 ; 6	205:103:1*	79	100	0	37
Cu(histidine)$_2^+$ in zeolite Y	CH_3CN; 75; 24	1.5:1:−[g]	TON = 1421[h]	66	33	38
PS−NH_2−Cu−Sal[i]	CH_3CN; 50; 7	1352:676:1*	77	70	30	39

[a]Molar ratios of TBHP/BzOH/M with M = metal (*) or catalyst (**). [b]The oxidant solution was 80% in di-*tert*-butyl peroxide. [c]Not mentioned. [d]Poly(S-DVB) = cross-linked chloromethylated poly(styrene−divinylbenzene). [e]PS = polystyrene, PBIM = diacetatobis(2-pyridylbenzimidazole), QBIM = diacetatobis(2-quinolylbenzimidazole). [f]H_2L = 2-[(2-hydroxy-phenylimino)-methyl]-4-(4-chloro-3-nitro-phenylazo)-phenol. [g]Referred as 0.75 Cu per unit cell. [h]Turnover number. [i]Polymer anchored Schiff base copper complex where PS-NH_2 is amino-polystyrene and Sal is salicylaldehyde.

same catalytic results at 24 h (entries 3 and 7, Table 2), further supporting the good catalyst stability of **1** and **2**.

CONCLUSION

In this work we demonstrated how the compositional diagram triangle can be employed for studying copper−molybdate hybrid solids. The approach has contributed to our understanding of the relationship between initial reagent concentration/stoichiometry and the resultant crystal structures. Three compounds, $[Cu^{II}_2(tr_2ad)_4](Mo_8O_{26})$ (**1**), $[Cu_4^{II}(\mu_4\text{-}O)(tr_2ad)_2(MoO_4)_3]\cdot 7.5H_2O$ (**2**), $[Cu^{I}_2(tr_2ad)_2](Mo_2O_7)\cdot H_2O$ (**3**), having extended 2D layered motifs, were characterized. The dinuclear and tetranuclear Cu^{II} clusters of **1** and **2**, respectively, exhibit quite different patterns for the magnetic exchange interactions. Whereas compound **1** shows only a minor magnetic exchange interaction of ferromagnetic nature between Cu^{II} pairs, compound **2** reveals appreciable overall antiferromagnetic interactions resulting in a singlet ground state. Compounds **1** and **2** show high thermal and chemical stability and were examined as catalysts in the epoxidation of *cis*-cyclooctene and in the oxidation of benzyl alcohol with different types of oxidants. The results obtained suggest that **1** and **2** are favorable heterogeneous catalysts for the synthesis of benzoic acid from benzyl alcohol. We believe that the proposed synthetic strategy could be used for the reinvestigation of many multicomponent hybrid systems, leading to new knowledge and technology.

ASSOCIATED CONTENT

Supporting Information

Crystallographic data (including data in CIF format), experimental details for X-ray structural analyses, spectral characterization data, and synthetic features. This material is available free of charge via the Internet at http://pubs.acs.org.

AUTHOR INFORMATION

Corresponding Authors

*E-mail: ab_lysenko@univ.kiev.ua.

*E-mail: liu@dcb.unibe.ch.

Notes

The authors declare no competing financial interest.

ACKNOWLEDGMENTS

Financial support by Deutsche Forschungsgemeinschaft, by the Ukrainian education program "Education, Training of students, PhD students, scientific and pedagogical staff abroad" (No.2201250), and by the Swiss National Science Foundation (Grant 200021-147143) is gratefully acknowledged. The Portuguese group is grateful to the Fundação para a Ciência e a Tecnologia (FCT), QREN, Fundo Europeu de Desenvolvimento Regional (FEDER), COMPETE, the European Union (EU), and the Associate Laboratory CICECO (PEst-C/CTM/LA0011/2013) for continued support and funding. The FCT and the EU are acknowledged for a postdoctoral grant to P.N. (SFRH/BPD/73540/2010) co-funded by MCTES and the European Social Fund through the program POPH of QREN.

DEDICATION

In memory of Professor Alexander Chernega.

REFERENCES

(1) (a) Hagrman, P. J.; Hagrman, D.; Zubieta, J. *Angew. Chem., Int. Ed.* **1999**, *38*, 2638−2684. (b) Rarig, R. S., Jr.; Zubieta, J. *J. Chem. Soc., Dalton Trans.* **2001**, *23*, 3446−3452. (c) Hagrman, P. J.; Zubieta, J. *Inorg. Chem.* **2000**, *39*, 5218−5224.

(2) bipy: Rarig, R. S., Jr.; Lam, R.; Zavalij, P. Y.; Ngala, J. K.; LaDuca, R. L., Jr.; Greedan, J. E.; Zubieta, J. *Inorg. Chem.* **2002**, *41*, 2124−2133.

(3) phen: Hagrman, P. J.; Zubieta, J. *Inorg. Chem.* **1999**, *38*, 4480−4485.

(4) triazole: (a) Zang, H.-Y.; Lan, Y.-Q.; Yang, G.-S.; Wang, X.-L.; Shao, K.-Z.; Xu, G.-J.; Su, Z.-M. *CrystEngComm* **2010**, *12*, 434−445. (b) Tian, A.-X.; Liu, X.-J.; Ying, J.; Zhu, D.-X.; Wang, X.-L.; Peng, J. *CrystEngComm* **2011**, *13*, 6680−6687. (c) Gong, Y.; Wu, T.; Jiang, P. G.; Lin, J. H.; Yang, Y. X. *Inorg. Chem.* **2013**, *52*, 777−784. (d) Dong, B.-X.; Xu, Q. *Inorg. Chem.* **2009**, *48*, 5861−5873. (e) Zhu, M.; Su, S.-Q.; Song, X.-Z.; Hao, Z.-M.; Song, S.-Y.; Zhang, H.-J. *Dalton Trans.* **2012**, *41*, 13267−13270.

(5) (a) Halasyamani, P.; Willis, M. J.; Stern, C. L.; Lundquist, P. M.; Wong, G. K.; Poeppelmeier, K. R. *Inorg. Chem.* **1996**, *35*, 1367−1371. (b) Halasymani, P. S.; Heier, K. R.; Norquist, A. J.; Stern, C. L.; Poeppelmeier, K. R. *Inorg. Chem.* **1998**, *37*, 369−371. (c) Norquist, A. J.; Heier, K. R.; Stern, C. L.; Poeppelmeier, K. R. *Inorg. Chem.* **1998**, *37*, 6495−6501. (d) Guillory, P. C. R.; Kirsch, J. E.; Izumi, H. K.; Stern, C. L.; Poeppelmeier, K. R. *Cryst. Growth Des.* **2006**, *6*, 382−389.

(6) Albrecht, T. A.; Stern, C. L.; Poeppelmeier, K. R. *Inorg. Chem.* **2007**, *46*, 1704−1708.

(7) Mahenthirarajah, T.; Li, Y.; Lightfoot, P. *Dalton Trans.* **2009**, *17*, 3280−3285.

(8) Cadiau, A.; Martineau, C.; Taulelle, F.; Adil, K. *J. Fluorine Chem.* **2013**, *150*, 104−108.

(9) (a) Kim, J.-Y.; Norquist, A. J.; O'Hare, D. *Chem. Mater.* **2003**, *15*, 1970−1975. (b) Doran, M. B.; Norquist, A. J.; O'Hare, D. *Inorg. Chem.* **2003**, *42*, 6989−6995. (c) Thomas, P. M.; Norquist, A. J.; Doran, M. B.; O'Hare, D. *J. Mater. Chem.* **2003**, *13*, 88−92.

(10) Fernández de Luis, R.; Urtiaga, M. K.; Mesa, J. L.; Larrea, E. S.; Rojo, T.; Arriortua, M. I. *CrystEngComm* **2012**, *14*, 6921−6933.

(11) Pope, M. T.; Müller, A. *Polyoxometalate Chemistry From Topology via Self-Assembly to Applications*; Kluwer Academic: Dordrecht, The Netherlands, 2001.

(12) Lysenko, A. B.; Senchyk, G. A.; Lincke, J.; Lässig, D.; Fokin, A. A.; Butova, E. D.; Schreiner, P. R.; Krautscheid, H.; Domasevitch, K. V. *Dalton Trans.* **2010**, *39*, 4223−4231.

(13) (a) Senchyk, G. A.; Lysenko, A. B.; Krautscheid, H.; Domasevitch, K. V. *Inorg. Chem. Commun.* **2011**, *14*, 1365−1368. (b) Sharga, O. V.; Lysenko, A. B.; Handke, M.; Krautscheid, H.; Rusanov, E. B.; Chernega, A. N.; Krämer, K. W.; Liu, S.-X.; Decurtins, S.; Bridgeman, A.; Domasevitch, K. V. *Inorg. Chem.* **2013**, *52*, 8784−8794.

(14) Aromí, G.; Barrios, L. A.; Roubeau, O.; Gamez, P. *Coord. Chem. Rev.* **2011**, *255*, 485−616.

(15) (a) Senchyk, G. A.; Lysenko, A. B.; Rusanov, E. B.; Chernega, A. N.; Krautscheid, H.; Domasevitch, K. V. *Inorg. Chim. Acta* **2009**, *362*, 4439−4448. (b) Senchyk, G. A.; Lysenko, A. B.; Boldog, I.; Rusanov, E. B.; Chernega, A. N.; Krautscheid, H.; Domasevitch, K. V. *Dalton Trans.* **2012**, *41*, 8675−8689. (c) Senchyk, G. A.; Lysenko, A. B.; Rusanov, E. B.; Chernega, A. N.; Jezierska, J.; Domasevitch, K. V.; Ozarowski, A. *Eur. J. Inorg. Chem.* **2012**, *35*, 5802−5813.

(16) (a) Kahn, O. *Molecular Magnetism*; VCH: Weinheim, Germany, 1993. (b) Pilkington, M.; Decurtins, S. *Chimia* **2000**, *54*, 593−601. (c) Bonadio, F.; Senna, M.-C.; Ensling, J.; Sieber, A.; Neels, A.; Stoeckli-Evans, H.; Decurtins, S. *Inorg. Chem.* **2005**, *44*, 969−978. (d) In *Magnetism—Molecular and Supramolecular Perspectives*; Thompson, L. K., Ed.; Coordination Chemistry Reviews; Elsevier: New York, 2005; Vol. *249*, pp 2549−2730.

(17) (a) *Stoe & Cie. X-SHAPE. Revision 1.06*; Stoe & Cie GmbH: Darmstadt, Germany, 1999. (b) *Stoe & Cie. X-RED. Version 1.22*; Stoe & Cie GmbH: Darmstadt, Germany, 2001.

(18) (a) Sheldrick, G. M. *Acta Crystallogr.* **1990**, *A46*, 467−473. (b) Sheldrick, G. M. *Acta Crystallogr.* **2008**, *A64*, 112−122.

(19) Brandenburg, K. *Diamond 2.1e*; Crystal Impact GbR: Bonn, 1999.

(20) (a) Moini, A.; Peascoe, R.; Rudolf, P. R.; Clearfield, A. *Inorg. Chem.* **1986**, *25*, 3782−3785. (b) Vilminot, S.; André, G.; Kurmoo, M. *Inorg. Chem.* **2009**, *48*, 2687−2692. (c) Vilminot, S.; André, G.; Richard-Plouet, M.; Bourée-Vigneron, F.; Kurmoo, M. *Inorg. Chem.* **2006**, *45*, 10938−10946. (d) Xu, Y.; Lu, J.; Goh, N. K. *J. Mater. Chem.* **1999**, *9*, 1599−1602. (e) Liu, P.; Liang, Y.; Lin, X.; Wang, C.; Yang, G. *ACS Nano* **2011**, *5*, 4748−4755. (f) Yang, H.; Jenkins, R. A.; Thompson, R. M.; Downs, R. T.; Evans, S. H.; Bloch, E. M. *Am. Mineral.* **2012**, *97*, 1977−1986. (g) Calvert, L. D.; Barnes, W. H. *Can. Mineral.* **1957**, *6*, 31−51. (h) Müller, A.; Krickemeyer, E.; Bögge, H.; Schmidtmann, M.; Kögerler, P.; Rosu, C.; Beckmann, E. *Angew. Chem., Int. Ed.* **2001**, *40*, 4034−4037. (i) Tian, C.; Wang, E.; Li, Y.; Xu, L.; Hu, C.; Peng, J. *J. Solid State Chem.* **2004**, *177*, 839−843.

(21) Restori, R.; Schwarzenbach, D. *Acta Crystallogr.* **1986**, *B42*, 201−208.

(22) Huang, Y.-Q.; Zhao, X.-Q.; Shi, W.; Liu, W.-Y.; Chen, Z.-L.; Cheng, P.; Liao, D.-Z.; Yan, S.-P. *Cryst. Growth Des.* **2008**, *8*, 3652−3660.

(23) Govor, E. V.; Lysenko, A. B.; Rusanov, E. B.; Chernega, A. N.; Krautscheid, H.; Domasevitch, K. V. *Z. Anorg. Allg. Chem.* **2010**, *636*, 209−217.

(24) (a) Drabent, K.; Bialonska, A.; Ciunik, Z. *Inorg. Chem. Commun.* **2004**, *7*, 224−227. (b) Drabent, K.; Ciunik, Z.; Chmielewski, P. J. *Eur. J. Inorg. Chem.* **2003**, *8*, 1548−1554.

(25) (a) Wang, Y.; Ding, B.; Cheng, P.; Liao, D.-Z.; Yan, S.-P. *Inorg. Chem.* **2007**, *46*, 2002−2010. (b) Senchyk, G. A.; Bukhan'ko, V. O.; Lysenko, A. B.; Krautscheid, H.; Rusanov, E. B.; Chernega, A. N.; Karbowiak, M.; Domasevitch, K. V. *Inorg. Chem.* **2012**, *51*, 8025−8033.

(26) Desiraju, G. R.; Steiner, T. In *The Weak Hydrogen Bond in Structural Chemistry and Biology*; Oxford University Press: Oxford, U.K., 1999.

(27) Hall, J. W.; Estes, W. E.; Estes, E. D.; Scaringe, R. P.; Hatfield, W. E. *Inorg. Chem.* **1977**, *16*, 1572−1574.

(28) Lorber, C. Y.; Smidt, S. P.; Osborn, J. A. *Eur. J. Inorg. Chem.* **2000**, *4*, 655−658.

(29) Jeyakumar, K.; Chand, D. K. *Open Catal. J.* **2008**, *1*, 6−10.

(30) http://www.alegesanatos.ro/dbimg/files/Benzyl%20Alcohol%20-%20Benzoic%20Acid.pdf.

(31) Brul, S.; Coote, P. *Int. J. Food Microbiol.* **1999**, *50*, 1−17.

(32) Araghi, M.; Ghorbani, A.; Yeganeh, F. E. *C. R. Chim.* **2013**, *16*, 109−113.

(33) Jaeger, B.; Stolle, A.; Scholz, P.; Mueller, M.; Ondruschka, B. *Appl. Catal., A* **2011**, *403*, 152−160.

(34) Valodkar, V. B.; Tembe, G. L.; Ravindranathan, A.; Ram, R. N.; Rama, H. S. *J. Mol. Catal. A: Chem.* **2004**, *208*, 21−32.

(35) Shilpa, M. L.; Gayathri, V. *Transition Met. Chem.* **2013**, *38*, 705−713.

(36) Shilpa, M. L.; Gayathri, V. *Transition Met. Chem.* **2013**, *38*, 53−62.

(37) Mobinikhaledi, A.; Zendehdel, M.; Safari, P. *React. Kinet., Mech. Catal.* **2013**, 1.

(38) Weckhuysen, B. M.; Verberckmoes, A. A.; Fu, L. J.; Schoonheydt, R. A. *J. Phys. Chem.* **1996**, *100*, 9456−9461.

(39) Islam, S. M.; Mondal, P.; Mukherjee, S.; Roy, A. S.; Bhaumik, A. *Polym. Adv. Technol.* **2011**, *22*, 933−941.